A NOVEL EXPERIMENTAL OBSERVATION OF THE GRAVITY-DRIVEN FLASHING OF METASTABLE WATER IN A HEATED POOL

Jimmy Martin[1,2], Pierre Ruyer[1], Matthieu Duponcheel[2], and Yann Bartosiewicz[2]
[1]Institut de Radioprotection et de Sûreté Nucléaire (IRSN), Saint-Paul-lez-Durance, 13115, France
[2]UCLouvain, Institute of Mechanics, Materials and Civil engineering, Louvain-la-Neuve, B-1348, Belgium

ABSTRACT

The gravity-driven flashing of superheated water, a non-equilibrium phase change phenomenon usually associated with geysers, has not been studied yet in the specific configuration of a pool heated from below. However, this vaporization mode is tightly linked with some of the safety issues of the Spent Fuel Pool (SFP) loss-of-cooling accident. In order to fill this gap, an experiment, presented in this article, was designed and provided first results that highlighted some relevant mechanisms behind this vaporization mode. By heating up 40 L of demineralized water at a constant reduced pressure of 25 mbar with a heating power of 1000 W, it was possible to reproduce the expected phenomenology at the laboratory scale. Starting the test with an initially large supersaturation in dissolved gases within the liquid, the latter, once superheated, vaporized onto the air nuclei that resulted from the liquid degassing. When the dissolved gases content dropped below a threshold value, the nucleation vanished. The liquid continued to heat-up for a while until an energetic equilibrium was reached between the heat supply and the heat removal induced by the free surface evaporation. This equilibrium substantially limited the superheats reached within the liquid.

KEYWORDS
Non-equilibrium phase change, dissolved gases, spent-fuel-pool, loss-of-cooling accident

1. INTRODUCTION

During a loss-of-cooling accident affecting a spent-fuel-pool (SFP)*, the overall decay heat of the fuels, potentially as high as a dozen megawatts, is no longer removed. In this situation, each stored spent fuel acts as a heat source and generates an upward flow of warm water named *plume*. A complex three-dimensional natural convection flow develops at pool scale [1], [2]. Gradually, the water heats up and vaporizes. If no countermeasures are taken during this transient, the pool level will drop down, ultimately leading to the uncovery of the spent fuels and later, to their degradation. Before that very outcome, the raise of the water temperature and the bubble nucleation mechanisms that may come into play could hinder the recovery of the SFP cooling by restarting the normal cooling systems, *e.g.* because of pump cavitation or loss of suction to the intake strainers within the basin [2]. In addition, the radioactive contamination initially retained in the water is expected to leak out and reach the atmosphere, on top of the pool. This release process is known as being triggered by the potential bubbling / boiling of the water containing the population of residual radionuclides [3].

Among the vaporization mechanisms that may occur during a SFP loss-of-cooling accident and lead to bubble formation is the gravity-driven flashing of superheated water, topic of the present paper. This phenomenon, usually associated to geysers [4], may be encountered in any system where an uprising hot fluid

*A spent-fuel-pool is generally 10-m deep, for an overall water volume of the order of 1000 m^3 [1].

experiences a significant decrease in hydrostatic pressure. For sufficiently large vertical systems, the fluid may exceed its *boiling point* (*i.e.* the saturation temperature) when flowing upwardly and reach a so-called *superheated* metastable state. From that situation, when vaporization *nuclei* are present within the fluid or onto the system's immersed walls, be they non-condensible and/or vapor tiny bubbles, the superheated liquid may turn into vapor, a process named *flashing* [5]. In a SFP, the gravity-driven flashing is promoted by the large depth of the pool. Along the pool's height, the water saturation temperature exhibits a 20°C difference, of sufficient magnitude for envisioning the occurrence of the phenomenon (Figure 1). Many experiments have been carried out in the past in vertical pipes or ducts heated from below, *e.g.* [6] or [7], or in the unheated pool of a flash evaporator, *e.g.* [8], [9] or [10]. But to our knowledge and as admitted by the community [2], this phenomenon has not been studied yet in the specific configuration of a heated pool. This finding has motivated the experimental study discussed in the present article. Hereafter, we first describe the test device designed and operated in order to investigate the pool-related gravity-driven flashing at a laboratory scale (1:25). This work is part of a collaboration between the *IRSN* and the *Université catholique de Louvain* (UCLouvain, Belgium) on that very topic, initiated in 2018. The collaboration is in direct link with the IRSN's DENOPI project on spent-fuel-pool accidents [11]. One may note that, in this project, the gravity-driven flashing of superheated water is investigated too at a larger and integral scale within the so-called MIDI facility (overall scaling: 1:6 - distorted vertical scale: 1:3). Next in this article, we provide the reader with novel phenomenological observations, thereby allowing a first characterization of some key features behind this vaporization mode.

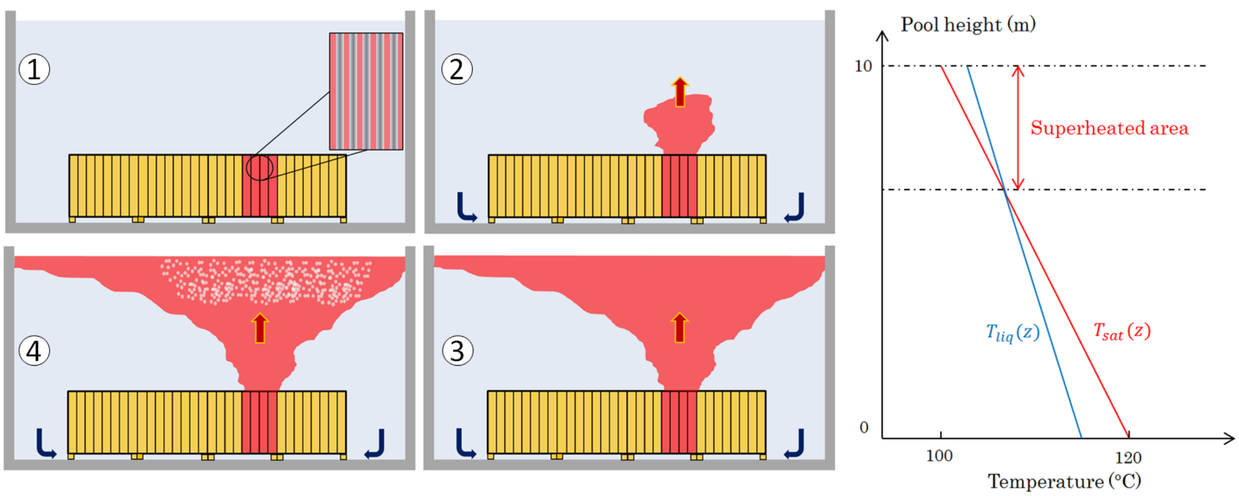

Figure 1. The envisioned gravity-driven flashing in a spent-fuel-pool under loss-of-cooling conditions. Left-hand-side: 1) Water is heated up by the spent fuels and keeps subcooled, 2) A natural convection flow develops at pool scale, 3) The boiling point is locally exceeded in the upper part of the pool by the uprising water, 4) The superheated water flashes and turns into bubbles. Right-hand-side: idealized vertical profile of the water temperature and of the boiling point within the uprising plume.

2. MATERIALS AND METHODS

2.1. Scaling and similarity

As introduced above, the discussed phenomenon is triggered by the vertical variation of the water saturation temperature, the latter resulting from the $1-\mathrm{bar}$ hydrostatic pressure difference along pool height, typically of the order of $10\ \mathrm{m}$. For obvious practical reasons, the study of the phenomenon cannot be considered at full scale. It is also impossible to reproduce that driving characteristics by an only scale reduction without compromises. Worse, if the mock-up scale is heavily reduced, the vertical saturation temperature difference might not be sufficient for preventing the onset of nucleate pool boiling onto the heating source, which in turn might hamper the gravity-driven flashing.

Interestingly, this issue can be solved by taking advantage from the particularity of water properties. Indeed, as one can notice from Figure 2, the variations of water saturation temperature T_{sat} are much steeper in the low-pressure range than around atmospheric pressure. This remarkable fact allows conserving the 20°C saturation temperature vertical difference of a SFP even at a reduced scale, with an appropriate choice of system's pressure. In a more general frame, this similarity approach may be beneficial to other types of applications where the gravity-driven flashing is expected, providing a way to reduce the size and hence the cost of the envisioned experiments and keeping water as the working fluid (*e.g.* for 1D-geyser flows or passive system pools). Accordingly, the most suited operating pressure can be determined as follows. If a 20°C saturation temperature vertical difference is to be conserved such as in the present study, then:

$$[\Delta T_{sat}(z)]_{SFP} = [\Delta T_{sat}(z)]_{mockup} \tag{1}$$

$$\iff \left[\int_0^H \frac{\partial T_{sat}}{\partial P} dP\right]_{SFP} = \left[\int_0^H \frac{\partial T_{sat}}{\partial P} dP\right]_{mockup} \tag{2}$$

$$\iff \left[\int_0^H \frac{\partial T_{sat}}{\partial P} \rho g dz\right]_{SFP} = \left[\int_0^H \frac{\partial T_{sat}}{\partial P} \rho g dz\right]_{mockup} \tag{3}$$

If one assumes that the variations of the water density and the partial derivative of the pressure-dependent saturation temperature can be neglected along the vertical axis, this yields:

$$\left[\frac{\partial T_{sat}}{\partial P} \rho g H\right]_{SFP} = \left[\frac{\partial T_{sat}}{\partial P} \rho g H\right]_{mockup} \tag{4}$$

$$\iff \left[\frac{\partial T_{sat}}{\partial P}\right]_{mockup} = \frac{H_{SFP}}{H_{mockup}} \left[\frac{\partial T_{sat}}{\partial P}\right]_{SFP} \tag{5}$$

For investigating the phenomenon in a pool-type geometry, the choice of an homothetic scaling ratio of 1:25 has been made. The latter leads to a mock-up height of 40 cm. By applying the above approach, the conservation of the 20°C saturation temperature vertical difference along that height imposes to retain a 23 mbar operating pressure, as it can be seen in Figure 3. Then, the heat source needs to be down-scaled as well. With a scaling ratio of 1:25, conserving the typical power density of a SFP, of the order of a $10\ \mathrm{kW/m^3}$, yields a reduced heat power of 1 kW.

Inevitably, this scale reduction leads to some distortions. First, when reducing the dimensions of the pool, the ratio between the buoyancy and the dissipative forces (viscosity, conduction), triggering the natural convection flows developing in the liquid bulk, is clearly distorded. This ratio is the well-known *Rayleigh* number Ra. Recalling that Ra varies as the cubic power of the system's height, a scale reduction of 1:25 affects that number by a factor 1.5×10^4. Fortunately, the Ra characterizing the accidental natural convection flows in a SFP are expected to be of the order of 10^{13}, far above the threshold value equal to 10^6 in water, from which the convection is considered turbulent†. Thus, those flows are expected to remain turbulent

†This estimate is made with an arbitrary driving temperature difference $\Delta T = 1$°C, a thermal expansion coefficient $\beta = 2.07 \times 10^{-4}$ °C, a thermal diffusivity $\kappa = 1.43 \times 10^{-7}$ m²/s, a viscosity $\nu = 1.00 \times 10^{-6}$ m²/s, a height $h = 10$ m and recalling that $Ra = \frac{g\beta\Delta T h^3}{\nu\kappa}$.

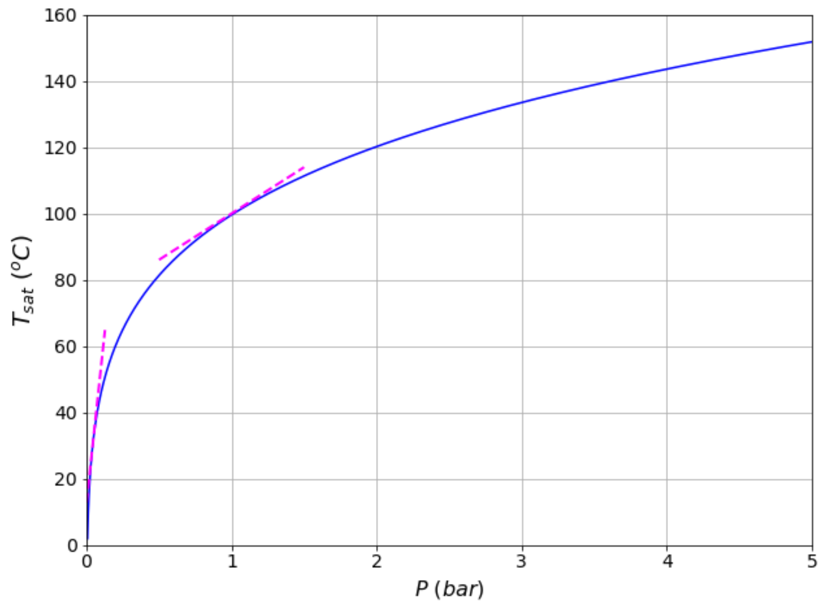

Figure 2. Variations of water saturation temperature T_{sat} against pressure. Note that those variations are steeper in the low-pressure range than around atmospheric pressure.

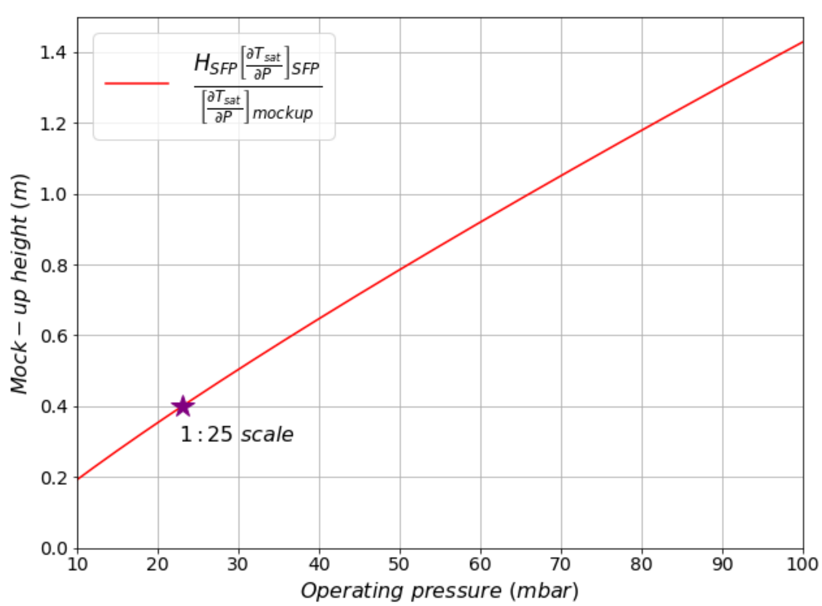

Figure 3. Relationship between the mock-up height and its operating pressure, ensuring the conservation of the 20^{o}C saturation temperature vertical difference of a SFP.

even at that reduced scale. Next, operating at a lower pressure distorts the bubbles typical size r by a factor 3.40 and the bubble area Σ by a factor 11.7. Indeed, bearing in mind that the ideal gas law is a good approximation of the behavior of water vapor for pressures below $50\ \mathrm{bar}$, then:

$$\frac{r_{mockup}}{r_{SFP}} = \left(\frac{P_{SFP}T_{mockup}}{T_{SFP}P_{mockup}}\right)^{1/3} \tag{6}$$

$$\frac{\Sigma_{mockup}}{\Sigma_{SFP}} = \left(\frac{P_{SFP}T_{mockup}}{T_{SFP}P_{mockup}}\right)^{2/3} \tag{7}$$

This last distortion will obviously affect the interfacial processes taking place between the superheated liquid and the gaseous phase and their inter-related heat and mass transfers are expected to be approximately 11.7 times bigger at that reduced scale. However, the bubble lifetime is oppositely affected by a scale reduction. In the present case, assuming that the order of magnitude of the bubble terminal velocity is weakly modified by the expected small distortion of the bubble size (*i.e.* 3.40), this lifetime is of the order of the scale ratio, *i.e.* 1:25. All in all, those two competing effects are expected to approximately compensate.

2.2. Characteristics

The experimental device, illustrated in Figures 4-5, that results from the above similarity approach consists in a 50 L closed vessel of height $H = 40\ \mathrm{cm}$, length $L = 45\ \mathrm{cm}$ and width $W = 30\ \mathrm{cm}$. The vessel is connected to a vacuum pump and a condenser. The vacuum pump allows imposing low pressure conditions down to $10\ \mathrm{mbar}$ within the gaseous upper volume of the vessel. Once those conditions are reached, the condenser keeps a constant pressure within this latter volume. As visible in Figure 6, working under those low pressure conditions yields a large vertical variation in the water saturation temperature at the scale of the test device, of the order of 20°C, thereby allowing a liquid heating at the bottom of the pool without boiling, as expected during a SFP loss-of-cooling accident. On that basis, it can be then envisioned to reach metastability conditions in the upper part of the pool, as the liquid rises by natural convection, and a subsequent phase change. A heating element, providing a $1\ \mathrm{kW}$ maximum thermal power to the water pool, is located at the bottom of the vessel. Its area represents 75% of the bottom surface. This electrically operated device is split into two separate parts, thereby allowing a spatially heterogeneous heating of the water. One may note that the specific arrangement of the heat source geometry in a SFP (*i.e.* the vertically stored nuclear fuel rod bundles) is not reproduced in this experiment, for simplicity. It is however represented in another and larger test facility devoted to SFP loss-of-cooling accidents, named MIDI, operated at IRSN [11]. Two parallel optical windows allow observing the phenomenon. At last, the right-hand-side inner vertical surface of the tank is made intentionally rough for promoting the production of flashing wall nuclei. Its measured arithmetical mean deviation R_a, an indicator of surface roughness, stands in between 2.9 and 3.2 µm, which corresponds to a maximum peak to valley height R_z of 12.5 µm. All immersed surfaces are made of stainless steel.

2.3. Instrumentation

The device is equipped with four Pt100 class A temperature probes whose position can be manually modified within the liquid bulk or its sky and with twelve Pt100 probes embedded in the lateral rough wall and in the heaters. Two pressure sensors are located on top of the tank for monitoring its boundary pressure with two complementing accuracy levels. One sensor is installed at its bottom-end, in order to deduce liquid mass variations throughout the tests. In addition, keeping in mind the potential importance of the dissolved gases for the studied phenomenon, an optical dissolved oxygen sensor (Hamilton VisiFerm™DO Arc 120)

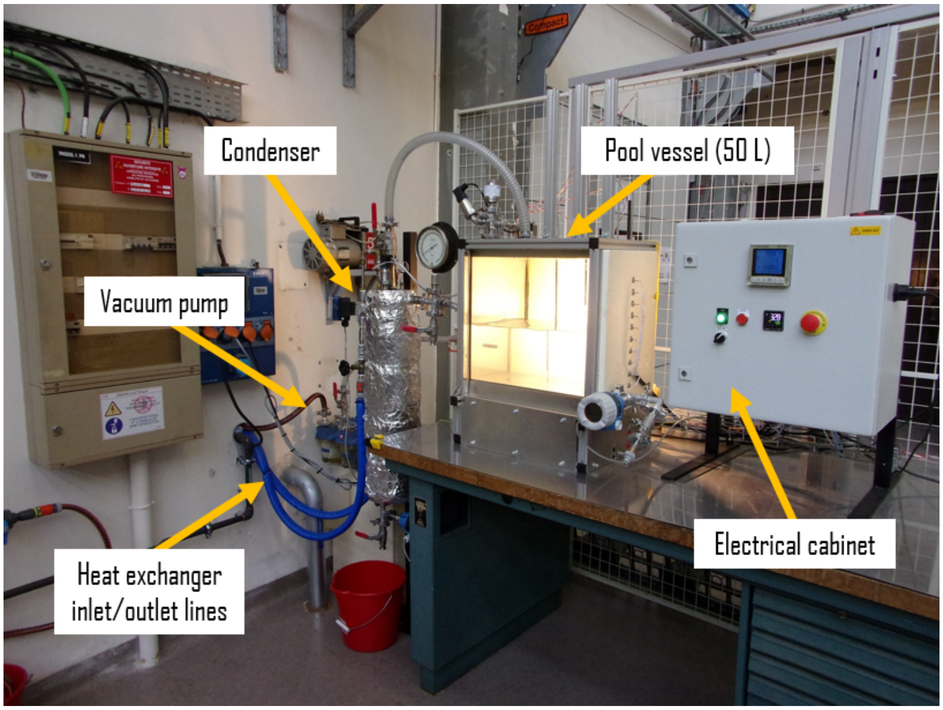

Figure 4. Overview of the test device designed and operated by IRSN / UCLouvain for investigating the gravity-driven pool flashing phenomenon at a laboratory scale.

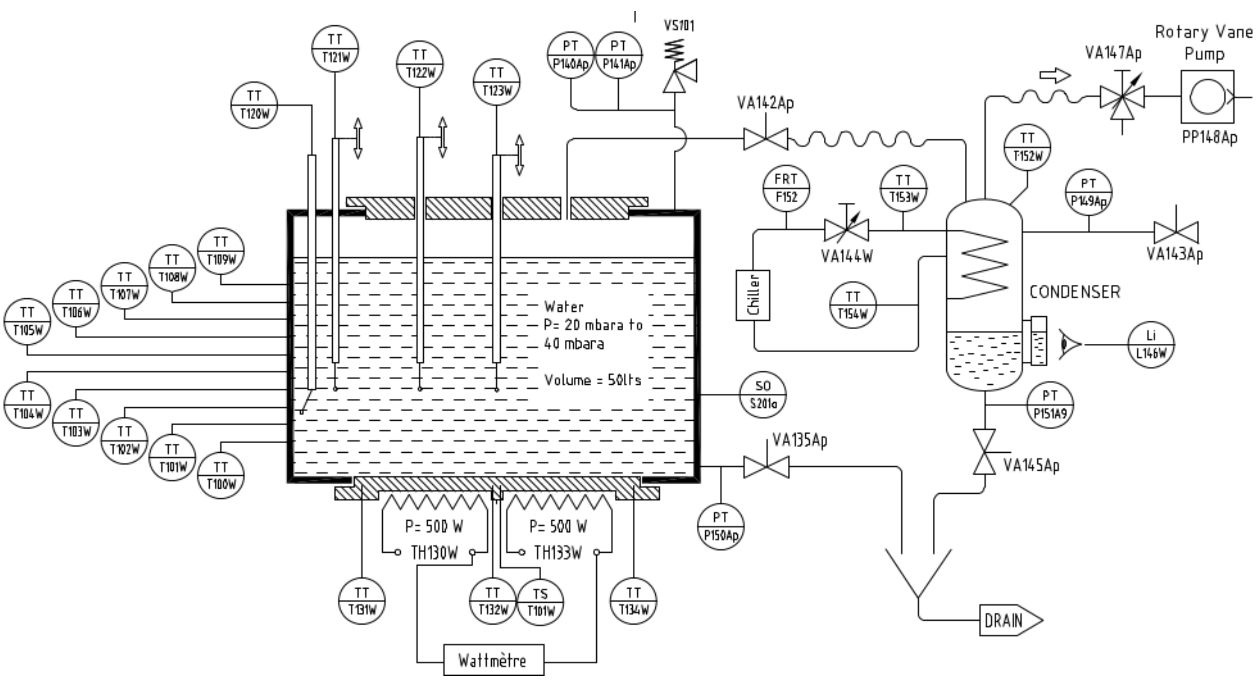

Figure 5. The experimental device layout and instrumentation.

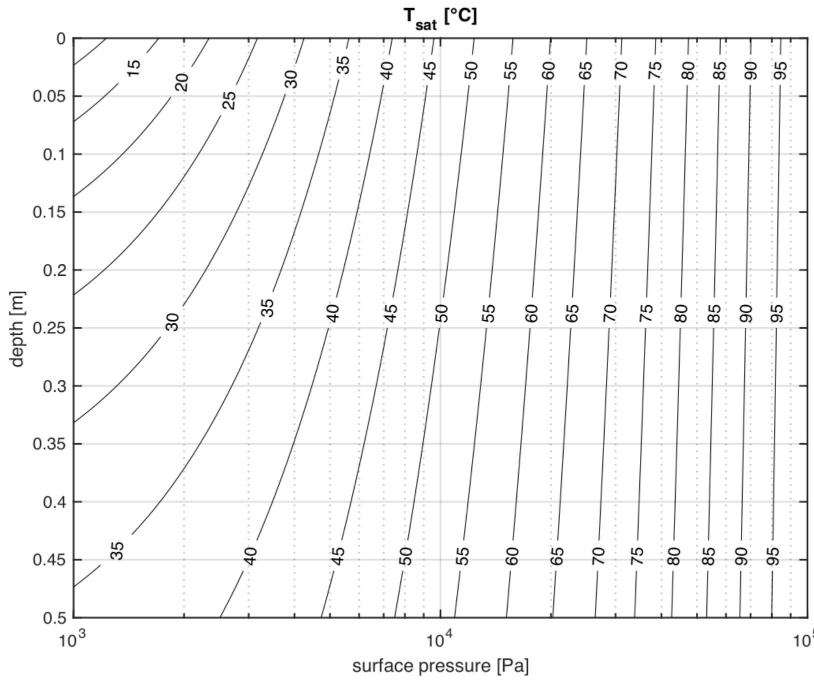

Figure 6. Vertical variation of the water saturation temperature within the pool against the atmospheric pressure. The lower the pressure, the bigger the vertical variation, thus allowing one heating the liquid at the bottom part of the pool without boiling.

measures the amount of oxygen within water. A FASTCAM™SA3 model 120K-M1 high-speed camera is occasionally placed in front of one of the two optical windows, thereby allowing recording the phenomena. The condenser is also instrumented in order to control and monitor the test conditions. It is equipped with two pressure sensors. One is located at its bottom-end and follows changes in its liquid inventory. One is installed at its top-end, in its gaseous volume, together with a temperature measurement. Two more temperature sensors are located at the inlet and outlet of the embedded heat exchanger. At last, a flow-meter provides the water mass flow rate circulating through the latter component.

2.4. Measurement uncertainties analysis

The uncertainties affecting the measurement results and the variables that are derived from those measurements were estimated following the recommendations of the *Guide to the expression of uncertainty in measurement* - or GUM - a reference guideline in metrology [12]. In details, the overall uncertainty affecting any result of the presented experiments is considered as deriving from two distinct, irreducible and unknown sources of errors. Those postulated errors are

- In link with the measurements performed throughout a test, any measuring chain being always intrinsically limited and imperfect ;
- In link with the experimental procedure and boundary conditions of the test device, applied throughout an experiment. In spite of the care taken in setting up and controlling a typical pool flashing test, the initial state and the boundary conditions of the experimental device, together with the actions taken

in the course of a test are expected to differ in some limited but irreducible extent, thereby bringing some more uncertainty to the test results.

The uncertainties which derive from the above first type of errors were estimated by means of any available information about the used measuring chain, such as for instance, the available calibration reports or sensor's technical data-sheet (those are hence Type B uncertainties, according to [12]). The uncertainties arising from the second type of errors are usually better estimated by means of statistical methods, in which case they are referred to as Type A uncertainties [12]. Those Type A uncertainties were highlighted by repeating 3 times a chosen reference test, by conserving at every trial the same experimental method, operator, equipment, environmental conditions and location. All in all, those differing uncertainties were propagated (if relevant) and then combined, with a coverage factor of 2 for the Type B and of 4.3 for the type A uncertainties (corresponding to the repeating of 3 tests). The obtained results, referring to the variables presented in the next section of this paper, are gathered in Table I.

Table I. The estimated Type A, Type B (expanded) and combined uncertainties affecting the presented results.

Variable name	Variable type	Type B ($k = 2$)	Type A ($k = 4.3$)	Combined
T_l	Liquid bulk temperature	0.024°C	0.52°C	0.52°C
T_g	Gas bulk temperature	0.024°C	0.55°C	0.55°C
P_g	Pool atmosphere total pressure	0.064 mbar	0.77 mbar	0.77 mbar
T_{sat}	Water saturation temperature	0.096°C	0.56°C	0.57°C
$\dot{Q}_p$	Heating power	1.8%	3%	3.5%
m_l	Pool liquid mass	0.160 kg	0.86 kg	0.87 kg
$\dot{m}_l$	Liquid vaporization rate	0.07 g/s	0.04 g/s	0.08 g/s
ΔT_{eq}	Non-equilibrium liquid temp. diff.	0.098°C	0.34°C	0.35°C
C_{O_2-eq}	O_2 concentration	2%	34%	34%
$\dot{C}_{O_2-eq}$	O_2 degassing rate	4%	34%	34%
L_{flash}/L	Dimensionless superheated length	1%	28%	28%

2.5. Experimental procedure

The pool-flashing experiments presented in this article were all achieved according to the following test procedure:

- **Filling stage**: the pool is filled up or partially drained, depending on the required initial water level ;
- **Bubbling stage**: the liquid pool is bubbled by means of the laboratory compressed air system, in order to reach a targeted and measured initial content in dissolved O_2 (if required) ;
- **Chiller start-up**: the chiller is parametrized and started-up, in order to reach a stationary cold source temperature prior to the test ;
- **Heaters start-up**: the required heat power is fixed by means of a rheostat and the heaters are then electrically fed → progressive increase of the liquid temperature, denoted as T_l, up to its targeted value ;

- **Depressurization**: once the required initial pool temperature is reached, the depressurization is initiated by starting up the vacuum pump. The vessel pressure naturally tends towards $P_{sat}(T_l)$, *i.e.* the saturation pressure corresponding to the initial liquid pool temperature T_l. At that stage, the pool atmospheric volume is quasi-exclusively filled with steam water and hence highly depleted in air (however, the liquid still contains some dissolved air) ;

- **Pressure regulation**: the vacuum pump is kept working throughout the test and the condenser heat exchanger valve is regulated by the operator (the cold source temperature set point being kept unchanged), both operations allowing the pool pressure to remain stable along the vaporization and degassing processes.

$\rightarrow$ Initiation of a pool flashing test at thermal saturation conditions, *i.e.* $T_l(t=0) = T_{sat}(P_g)$.

3. RESULTS AND DISCUSSION

3.1. The observation of a temporary gravity-driven flashing but long-lasting superheats

This first observation was obtained under the following initial conditions, that are as similar as possible from the reference SFP parameters discussed above:

- **Downscaled thermal power**: 1 kW ;
- **Downscaled pressure**: 25 mbar ;
- **Downscaled initial pool level**: 30 cm ;
- **Initial content in dissolved oxygen**: 6.5 mg/L (value in excess at a pressure of 25 mbar).

Starting the test under thermal saturation conditions and with an excess in dissolved gases, the thermodynamic system constituted by the liquid pool evolved according to a two-stage process. During the first stage which lasted approximately 45 min, a strong and continuous bubbling was observed below the water free surface, as represented in Figure 7. This latter process gradually weakened over time, yielding fewer but bigger bubbles, as visible in Figure 8, which is a picture of the pool, taken at time $t = 30$ min. It is also worth noting that the initial strong bubbling appeared, during the first 3 min of the test, as originating from numerous gaseous *nuclei*, formed onto the immersed wall surfaces of the pool. However, for the remaining period till the regime transition, the origin of the gaseous *nuclei* yielding the bubbly flashing visible in Figure 8 is for now unclear, although, as a first guess, we can assume those *nuclei* as coming from foreign solid particles suspended in the liquid [13]. Then, after about 45 min, a second regime characterized by a quasi-absence of bubble nucleation settled. Around the end of the test, the observation of nucleation became a rare but violent event. Indeed, at that very moment, the latter occurred randomly and was understood as resulting from the fortuitous release of non-condensible gas bubbles that remained temporarily attached to the immersed walls or from the shock of liquid droplets falling down from the top of the pool vessel. This uncommon process was recorded during a preliminary pool flashing test by means of the high-speed camera equipping the device and is illustrated in the below Figure 9. Most often, the burst of decametric bubbles at the water free surface such as the one illustrated herein led to the generation of secondary tiny bubbles by gas entrapment at that very surface, thus sustaining the flashing of superheated water during a brief period before the phenomenon vanished. Such secondary bubbles are visible underneath the free surface in the last three pictures of Figure 9. On the other hand, the high intensity associated with this brief vaporization resulted from the high superheating reached within the liquid around the end of the test, as discussed in what follows.

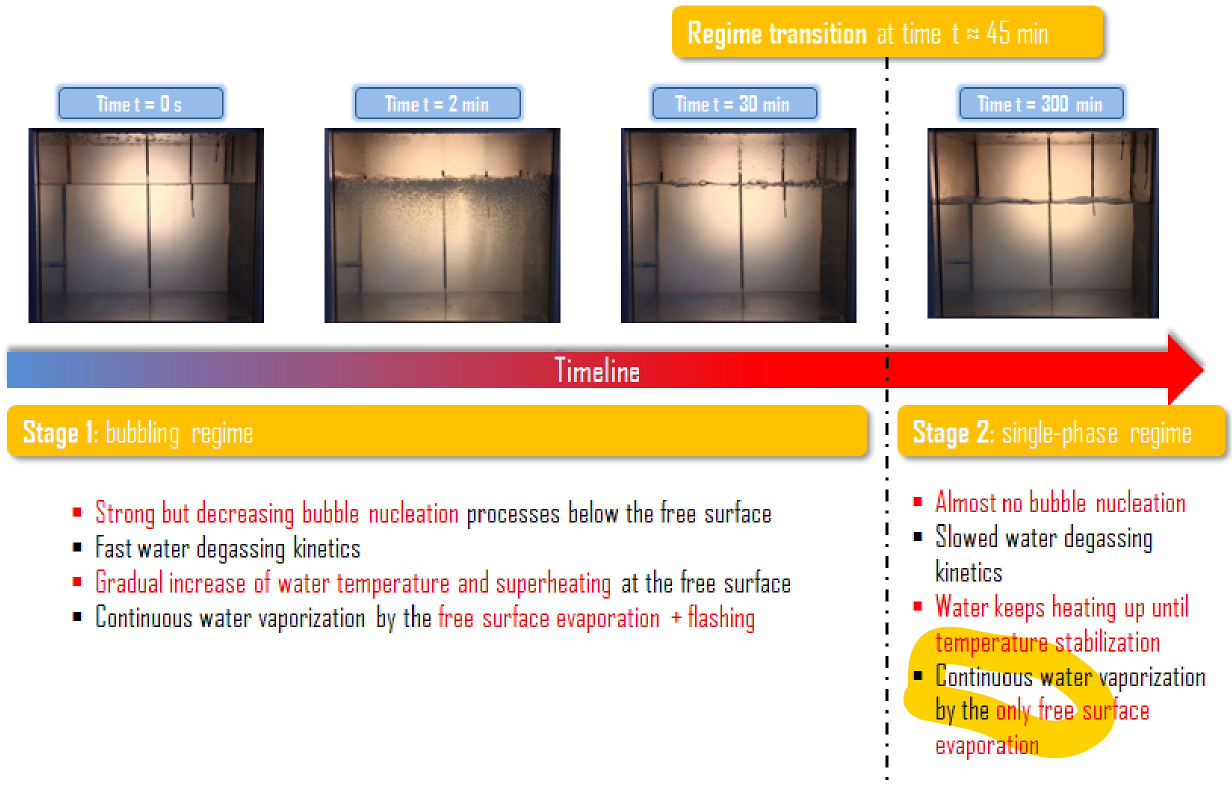

Figure 7. The two-stage gravity-driven flashing of superheated water observed within the test device, when starting the experiment at thermal saturation and with an excess in dissolved gases.

Overall, the measurements performed throughout the experiment were consistent with this ~~phenomenological picture~~ and exhibited some specific patterns. At the startup of the test, as seen in Figure 10, T_l, the measured liquid pool temperature was initially equal to $T_{sat}(P)$, the saturation temperature, computed from the pool atmosphere pressure measurement $P = P_g$ and the following correlation

$$T_{sat} = \frac{5120}{13.7 - \text{Log}\left(\frac{P}{1000}\right)} - 273.15 \tag{8}$$

where P is given in mbar and T_{sat} in °C. One may also notice that T_g, the pool atmosphere temperature measurement was approximately equal to T_{sat} throughout the test, thereby indicating that the pool gaseous volume was almost fully filled with water vapor. As visible in the right-hand-side of Figure 10, the pool pressure P_g varied slightly and negligibly along the experiment. The thermal power provided by the heat source led to a gradual water heating in its metastable domain, as depicted in the left-hand side graph of Figure 11, where

$$\Delta T_{eq} = T_l - T_{sat}(P_g) \tag{9}$$

represents the so-called *liquid thermal metastability degree* [14], here evaluated at the water free surface. From $t = 3.5$ hrs, ΔT_{eq} stabilized at a value of 5°C ±0.35°C up to the end of the test.

Figure 8. During the first stage of the test and after the initial strong bubbling originating from the immersed walls, the superheated water continuously flashed and turned into bubbles just below the liquid free surface.

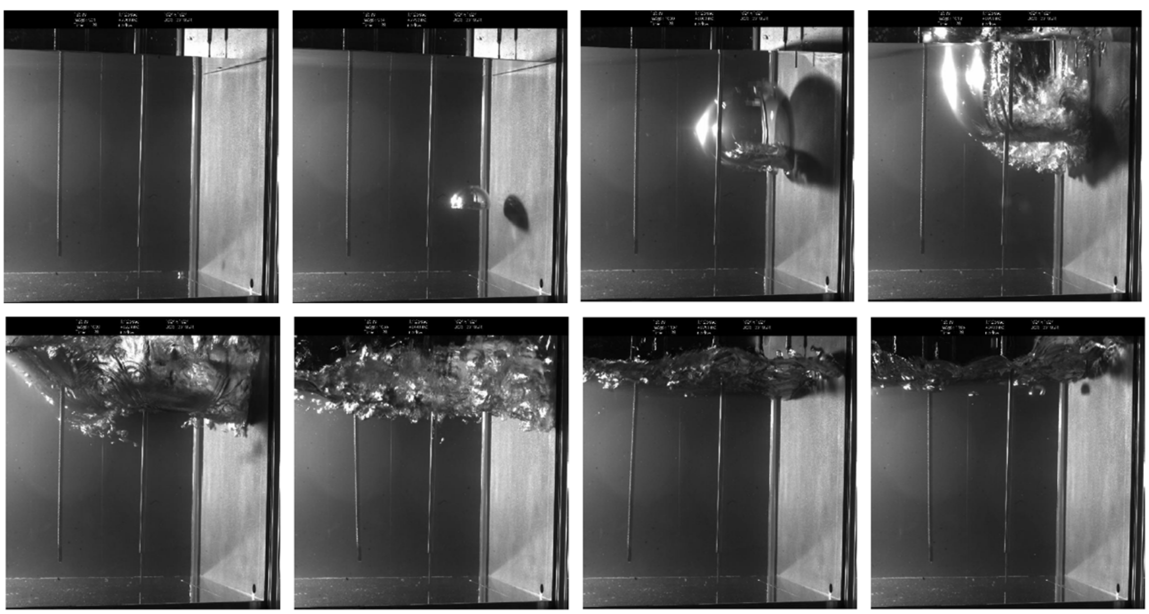

Figure 9. Around the end of the test, high superheats of the order of 5°C were reached below the liquid free surface and the phenomenon became very sensitive to any perturbation. Here, an air bubble originating from the bottom of the tank led to the violent vaporization of metastable water.

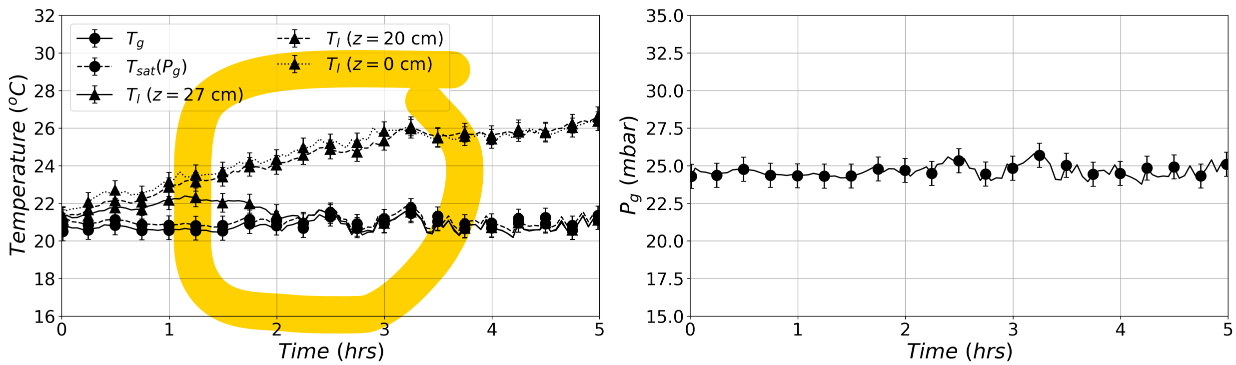

Figure 10. Left: measured fluid temperatures (the heights z mentioned in the legend for each liquid measurement T_l correspond to the sensor location, with $z = 0$ being the location of the pool bottom surface). Right: measured pressure within the pool atmosphere.

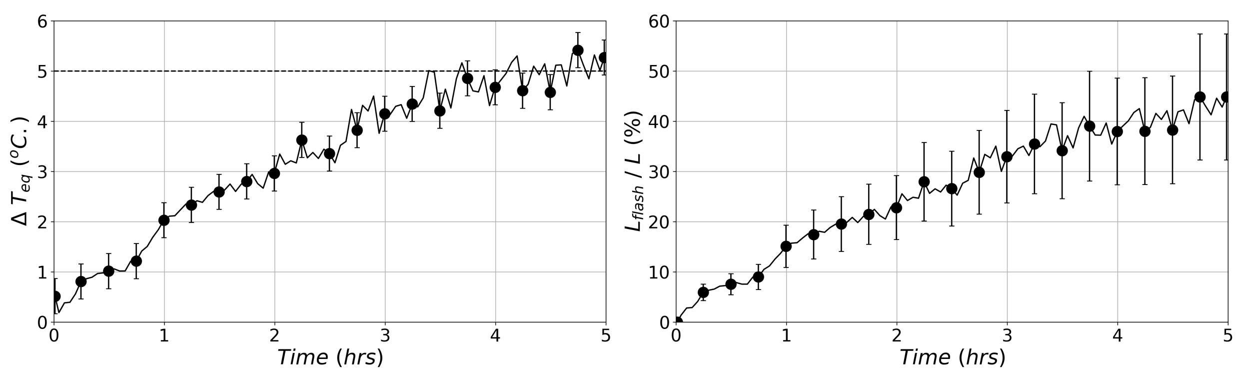

Figure 11. Left: the time-~~trend~~ of thermal metastability degree of the heated liquid. Right: ~~the length of the liquid bulk superheated area located below the free surface was an increasing function of time.~~

In Figure 12, the left-hand-side graph is the liquid water mass m_l and the right-hand-side represents its time-derivative $\dot{m}_l$. In the left graph, the water mass was determined on the basis of the simultaneous pressure measurements performed at the pool upper and lower ends and the prior characterization of the relationship between m_l and the measured hydrostatic pressure difference $\Delta P_{z;pool}$. The achieved device qualification tests yielded the following correlation

$$m_l = 1.39\,\Delta P_{z;pool} + 0.60 \tag{10}$$

Further, one can approximate the liquid vaporization rate as

$$\dot{m}_l \approx \frac{m_l(t+\Delta t) - m_l(t)}{\Delta t} \tag{11}$$

As one can notice, the water rapidly vaporized at an increasing rate $\dot{m}_l$, which eventually stabilized to

$$\dot{m}_l \approx \frac{\dot{Q}_p}{h_{gsat}(P_g)} = 0.4\ \mathrm{g/s} \tag{12}$$

where $\dot{Q}_p$ is the heat power and $h_{gsat}(P_g)$ the water vapor specific enthalpy at saturation. This interesting fact is the positive consequence of the pressure-based similarity approach proposed in this article. Indeed, working here at such a reduced pressure of $25\ \mathrm{mbar}$ imposes to the system a mild level of working temperatures, of the order of 25°C, thereby minimizing the heat losses at the pool boundaries. At that period of the test and in agreement with the absence of any sustained bubble nucleation, one may assert that the free surface evaporation of the liquid was the only vaporization mode allowing to energetically compensate for the heat supplied at the bottom of the pool.

As envisioned, the liquid bulk superheating was restricted to a limited upper area of the pool (*cf.* Figure 8, bubbles nucleated only below the free surface during the first stage of the test). As depicted in Figure 1, this area is expected to be bounded by the free surface and by the location at which the vertical profiles of the liquid temperature $T_l(z)$ and of the saturation temperature $T_{sat}(z)$ intersect. Reasonably assuming that the vertical liquid temperature T_l is constant (*cf.* Figure 10, the measured liquid temperatures did not differ much from each other) and based on the pressure measurements performed throughout the test at the lower and upper parts of the pool, the length of this superheated area L_{flash} can be approximated as follows

$$\frac{L_{flash}}{L} \approx \frac{T_l - T_{sat}(z=L)}{T_{sat}(z=0) - T_{sat}(z=L)} \tag{13}$$

where, L is the estimated collapsed level of the liquid pool, $T_{sat}(z=0)$ and $T_{sat}(z=L)$ are the saturation temperature, respectively estimated at the pool free surface and at its bottom end. In the above expression, the saturation temperatures are estimated with Equation (8) and the collapsed level is deduced from Equation (10) as follows

$$L = \frac{1}{S_p\,\rho_l}\,(1.39\,\Delta P_{z;pool} + 0.60) \tag{14}$$

in which S_p is the liquid free surface area, equal to $0.135\ \mathrm{m}^2$ and ρ_l, is the liquid density, estimated from T_l and P_g. The obtained result is plotted in the right-hand-side of Figure 11. As one can see, that length, initially null, increased over time and eventually represented about 45% of the pool collapsed level.

Next, the left-hand-side graph represents the direct measurement of the dissolved oxygen concentration within the liquid C_{O_2}, which indicates the amount of dissolved air throughout the test despite the absent

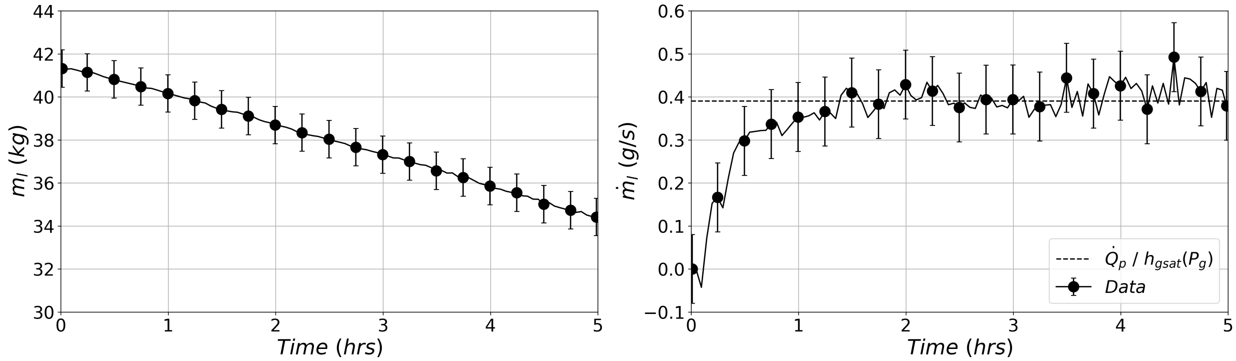

Figure 12. Left: estimated liquid mass m_l. Right: estimated liquid vaporization rate $\dot{m}_l$.

measurement of the other main contributor to the air composition: the N_2 species. The right-hand-side graph is an estimate of the O_2 degassing flux $\dot{C}_{O_2}$, given by

$$\dot{C}_{O_2} \approx \frac{C_{O_2}(t+\Delta t) - C_{O_2}(t)}{\Delta t} \tag{15}$$

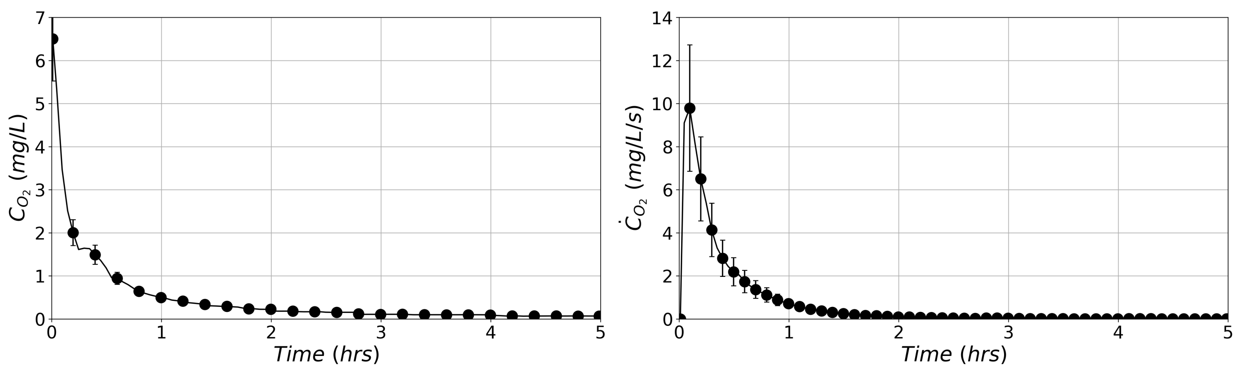

Figure 13. Left: measured dissolved oxygen concentration C_{O_2}. Right: estimated oxygen degassing rate $\dot{C}_{O_2}$.

It is worth pointing out that the O_2 degassing flux, which was almost null initially, peaked temporarily at a value of approx. $10\ \mathrm{mg/L/s}$, before dropping back to low values, from $t = 60\ \mathrm{min}$. It suggests the existence of a substantial mass transfer within the liquid pool, restricted to the initial phase of the test. This result is in agreement with the pool visualization performed at some key moments of the test, which revealed an initial strong bubbling process (Figures 7-8). The bubbling being known as efficiently promoting the heat and mass transfers in a liquid [15], it is hence an interesting candidate for explaining the observed trend in $\dot{C}_{O_2}$.

3.2. The key role played by the presence of dissolved gases highlighted

As evidenced above, the present experimental conditions promoted some bubble nucleation only during a first stage of the test, which here lasted approximately $45\ \mathrm{min}$. Paradoxically, this sustained bubbling ended while the liquid superheats were substantially high. The only variables which correlated well in time with this peculiar observation are the dissolved oxygen concentration C_{O_2} and its associated degassing rate $\dot{C}_{O_2}$.

Indeed, from Figure 13, one may notice that most of the degassing occurred during the first hour of the test, *i.e.* when the liquid was strongly bubbling. Around the transition time, the oxygen concentration dropped below approximately $0.7\ \mathrm{mg/L}$ and so did the oxygen supersaturation ΔC_{O_2-eq}, expressed as

$$\begin{aligned} \Delta C_{O_2-eq} &= C_{O_2} - C_{O_2-eq} \\ &\approx C_{O_2} \end{aligned} \tag{16}$$

with C_{O_2-eq}, the dissolved oxygen concentration value corresponding to the equilibrium between the latter dissolved gas and its counterpart within the pool atmosphere. Here $C_{O_2-eq} \approx 0$ because, as seen in Figure 10, the pool atmosphere remained almost filled with water vapor throughout the test. Thus, the oxygen partial pressure in this volume was necessarily close to zero. Therefore, the occurrence of the observed bubble nucleation required an initial dissolved gases supersaturation bigger than some threshold value. This suggests that the presence of dissolved gases within the liquid is the key factor triggering the bubbly flashing of superheated water in a pool-type geometry. If this hypothesis is correct, starting another test with a high depletion in dissolved gases would reduce the duration of the bubbling period and in turn, speed up the reach of the final, free-surface-evaporation-based, energetic equilibrium. In order to verify this hypothesis, we performed such a test starting with an initial dissolved oxygen of $C_{O_2}(t=0) = 0.15\ \mathrm{mg/L}$, *i.e.* well below the threshold value identified above. For getting that specific initial state, we boiled up and degassed a large amount of water at low pressure, a day before. The pool vessel was then kept isolated from the experimental hall atmosphere during the night. In doing so, the depleted water was left in the only contact of the pool inner atmospheric volume, full of steam, and did not re-gassed that much. The next day, the pool was briefly re-pressurized at atmospheric pressure and the excess of liquid was removed down to the required initial pool level of $30\ \mathrm{cm}$, prior to the launch of the experiment.

The obtained results are plotted in Figure 14. As one can see, the interpretation proposed above matches well with the data. Indeed and as expected, by starting the test with almost no dissolved gases, the system rapidly tended toward the free-surface-evaporation-based energetic equilibrium, corresponding to a maximum metastability degree of 5°C. Except the rare events discussed in the previous section, no bubble nucleation was observed at all in this additional test. Interestingly, this reached thermal metastable state was pretty stable and long-lasting. It lasted here approximately $4\ \mathrm{hrs}$ whereas the cleanliness of the water used was not excessively controlled. This clearly highlights the presence of dissolved gases in the liquid as a key factor for a bubbly flashing in the present configuration. The investigation of the link between this result and the potential nucleation mechanisms taking place in the superheated liquid is left as a perspective of the present work.

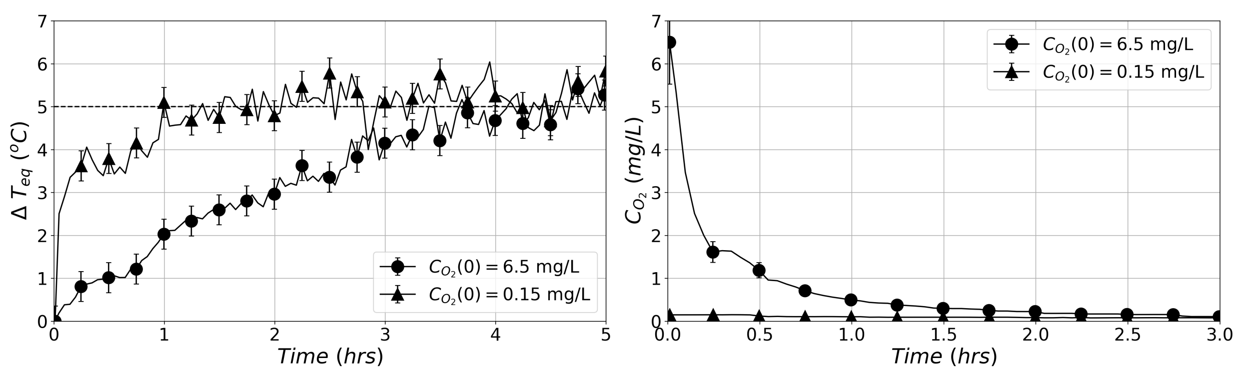

Figure 14. Left: compared liquid thermal metastability degrees ΔT_{eq}. Right: compared dissolved oxygen concentrations C_{O_2}.

4. CONCLUSION

In this article, we presented a novel gravity-driven flashing experiment with the aim to get a first insight into this physics in a pool heated from below. The test was intentionally performed starting from an initial excess of dissolved gases within the liquid bulk, for assessing the impact of the latter parameter. In the test, the liquid gradually heated up by natural convection, deviated from its thermodynamic equilibrium conditions and vaporized. A substantial area of metastable/superheated liquid built-up underneath the free surface. Consecutively, the liquid degassed, as evidenced by the dissolved oxygen concentration measurement. This phenomenology exhibited two distinct stages. During the first stage, the liquid pool was subjected to a strong bubbling process which here ended at a transition time of approximately 45 min. Ultimately a free-surface-evaporation-based energetic equilibrium was reached and the maximum liquid superheating stabilized around 5°C. Interestingly, this value remained pretty stable over a significant time period. The presence of some dissolved gases in the liquid prior to the test was shown as being the main contributor to the duration of the bubbly stage of the gravity-driven flashing in a pool-type geometry. As a future step, the phenomenon will be further investigated with a focus on the observed transition between the bubbling/non-bubbling regimes. For that purpose, the pool atmospheric pressure, which fixes too the initial pool liquid temperature, will be naturally varied within a range of values that still keeps preventing the boiling of water onto the heated bottom walls. The initial pool level is another parameter that fixes the local liquid pressure and will be varied as well. Most important, several initial liquid contents in dissolved gases will be investigated and the degassing process itself will be fully characterized. At last, the local hydrodynamics is known to play a role in the release of bubbles nucleated onto those nuclei [16]. By driving the power distribution between the two pool's heaters, more flow topologies will be set up, thereby allowing studying this effect in more details.

REFERENCES

1. OECD/NEA, "Status report on spent Fuel Pools under Loss-of-Cooling and Loss-of-Coolant Accident Conditions," (2014).

2. OECD/NEA, "Phenomena Identification and Ranking Table : R&D Priorities for Loss-of-Cooling and Loss-of-Coolant Accidents in Spent Nuclear Fuel Pools," (2018).

3. A. Wassel, A. Mills, D. Bugby, and R. Oehlberg, "Analysis of radionuclide retention in water pools," *Nuclear Engineering and Design*, **90**, pp. 87–104 (1985).

4. X. Lu and A. Watson, "A review of geysering flows," *Proc. Proc. 24th NZ Geothermal Workshop*, (2002).

5. Y. Liao and D. Lucas, "Computational modeling of flash boiling flows: A literature survey," *International Journal of Heat and Mass Transfer*, **111**, pp. 246–265 (2017).

6. A. L. Manera et al., "Stability of natural-circulation-cooled boiling water reactors during startup: experimental results," *Nuclear Technology*, **143**, pp. 77–88 (2003).

7. M. Furuya et al., "Flashing-induced density wave oscillations in a natural circulation BWR - mechanisms of instability and stability map," *Nuclear Engineering and Design*, **235**, pp. 1557–1569 (2005).

8. D. Saury, S. Harmand, and M. Siroux, "Flash evaporation from a water pool: Influence of the liquid height and of the depressurization rate," *International Journal of Thermal Sciences*, **44**, pp. 953–965 (2005).

9. S. Gopalakrishna, V. M. Purushothaman, and N. Lior, "An experimental study of flash evaporation from liquid pools," *Desalination*, **65**, pp. 139–151 (1987).

10. J. I. Kim and N. Lior, "Some critical transitions in pool flash evaporation," *International Journal of Heat and Mass Transfer*, **40**, pp. 2363–2372 (1997).

11. J. Martin, G. Brillant, C. Duriez, N. Trégourès, and C. Marquié, "The IRSN DENOPI project: a research program on spent-fuel-pool loss-of-cooling and loss-of-coolant accidents," *Proc. Proc. 17th NURETH conference*, Xi'an, Shaanxi, China, Sept. 3-8, (2017), ANS.

12. JCGM, "Guide to the expression of uncertainty in measurement," JCGM 100:2008, JCGM (2008).

13. C. Brennen, *Cavitation and bubble dynamics*, Cambridge University Press (2014).

14. P. Debenedetti, *Metastable Liquids: Concepts and Principles*, Princeton University Press (1996).

15. J. Lienhard IV and J. Lienhard V, *A Heat Transfer Textbook, fifth edition*, Phlogiston Press (2020).

16. T. Shin and O. Jones, "Nucleation and flashing in nozzles - 1," *International Journal of Multiphase flow*, **19**, pp. 943–964 (1993).